PHYSICAL REVIEW D **88,** 034503 (2013)

Phase diagram of Yang-Mills theories in the presence of a θ term

Massimo D'Elia*
Dipartimento di Fisica dell'Università di Pisa and INFN—Sezione di Pisa, Largo Pontecorvo 3, I-56127 Pisa, Italy

Francesco Negro†
Dipartimento di Fisica dell'Università di Genova and INFN—Sezione di Genova, Via Dodecaneso 33, I-16146 Genova, Italy
(Received 28 June 2013; published 20 August 2013)

We study the phase diagram of non-Abelian pure gauge theories in the presence of a topological θ term. The dependence of the deconfinement temperature on θ is determined on the lattice both by analytic continuation and by reweighting, obtaining consistent results. The general structure of the diagram is discussed on the basis of large-N considerations and of the possible analogies and dualities existing with the phase diagram of QCD in the presence of an imaginary baryon chemical potential.

DOI: 10.1103/PhysRevD.88.034503 PACS numbers: 11.15.Ha, 12.38.Aw, 12.38.Gc

I. INTRODUCTION

The possible presence of a nonzero θ parameter in the langrangian of QCD has been discussed for a long time. Such a parameter is coupled to the topological charge density,

$$\mathcal{L}_\theta = -i\theta q(x) = -i\theta \frac{g_0^2}{64\pi^2} \epsilon_{\mu\nu\rho\sigma} F^a_{\mu\nu}(x) F^a_{\rho\sigma}(x),$$

which violates P and CP symmetries, and its effects on the structure of non-Abelian gauge theories are intimately nonperturbative.

Experimental upper bounds on the parameter are quite stringent, $|\theta| \lesssim 10^{-10}$. Nevertheless, the dependence of QCD on θ is quite interesting, from both a theoretical and a phenomenological point of view; think for instance of the solution to the $U(1)_A$ problem, regarding the mass of the η' meson [1,2].

The study of θ-related issues is particularly interesting when one investigates the behavior of non-Abelian gauge theories at finite temperature T. Modifications in θ dependence are a probe of the changes in the nonperturbative properties of the theory and of the approach to the semiclassical regime expected at asymptotically high temperatures [3–5]. Topological charge fluctuations may be relevant—also from a phenomenological point of view—around the deconfinement transition, where local effective variations of θ may be detectable as event-by-event P and CP violations in heavy-ion collisions [6].

The purpose of the present paper is to discuss some general features of the phase diagram of pure SU(N) Yang-Mills theories in presence of a θ term. Unfortunately, the addition of such a term makes the Euclidean action complex, hindering direct numerical lattice simulations, as it happens for QCD at finite baryon chemical potential. For this reason, most of the present knowledge is based on model studies, on the computations of θ derivatives at $\theta = 0$, or on other methods which partially circumvent the sign problem like analytic continuation from imaginary chemical potentials [7–12].

In Ref. [11] we have already discussed the dependence of the critical deconfining temperature on θ, providing an estimate of this dependence in the large-N limit and a numerical computation for $N = 3$ based on analytic continuation from results obtained at imaginary values of θ, for which the action is real. The main result is that T_c decreases as a function of θ, being a linear function of θ^2 for small θ values: such a fact is in agreement with predictions coming from continuity-based semiclassical approximations [13–15] and model computations [16–19], and can be simply interpreted by considering that the free energy of the confined phase increases, as a function of θ, more than in the deconfined phase (since the topological susceptibility drops at T_c [20–22]), so that the deconfined phase becomes more and more favorable as θ increases [11].

The first purpose of the present study is to provide stronger numerical evidence regarding the determination of $T_c(\theta)$. In Sec. II A we present new data at imaginary θ on a finer lattice—corresponding to a temporal extent $N_t = 10$—which confirm the continuum limit extrapolation of Ref. [11], and in Sec. II B, we obtain an independent determination of $T_c(\theta)$ for small values of θ, based on a reweighting of data at $\theta = 0$, showing that it is consistent with the determination from imaginary θ, and hence that systematic effects are under control for both methods. Consistency between analytic continuation and reweighting will also be demonstrated for the dependence on θ of other physical observables, like the Polyakov loop.

A question which is naturally related to previous topics is how physical quantities depend on the topological sector Q, especially around the deconfinement transition. This issue, which is discussed in Sec. II C, is of particular interest for the related information about the systematic effects involved in numerical simulations carried out within a fixed topological sector, like those exploiting

*delia@df.unipi.it
†fnegro@ge.infn.it

overlap fermions. The problem has been investigated recently in the literature [23–25], showing that, for some quantities, systematic effects are well under control; see for instance Ref. [25] for a study regarding the pure gauge topological susceptibility at finite T. We will show that for other quantities like the Polyakov loop effects on finite volumes can be larger, especially around T_c, and that even small deviations of T_c itself are detectable when switching from one sector to the other.

In Sec. III, we will discuss the general properties of the phase diagram in the $T_c - \theta$ plane. Unfortunately, presently available numerical methods, like analytic continuation or reweighting, do not allow us to obtain much reliable information, apart from the curvature of the critical line $T_c(\theta)$ at $\theta = 0$. Therefore, part of the discussion is based on known large-N considerations and model predictions [26–35], as well as recent numerical evidence [36] regarding the change in the realization of θ dependence and periodicity, which takes place at the deconfinement transition. Particular emphasis will be placed on the analogy that we draw between the $T_c - \theta$ diagram and the phase diagram of QCD in the presence of an imaginary baryon chemical potential μ_B: we will speculate about the duality between the two diagrams, in the sense of an exchange between the high-T and the low-T regions, and about its possible relation with a duality of the relevant degrees of freedom. Finally, in Sec. IV we will draw our conclusions.

II. DEPENDENCE OF THE DECONFINING TEMPERATURE ON θ

Various model computations predict that the critical deconfining temperature in QCD decreases as the θ parameter is switched on [11,13–15,17–19]. The theory is CP-invariant for $\theta = 0$, and hence thermodynamical quantities and $T_c(\theta)$ itself are expected to be even functions of θ, i.e.,

$$\frac{T_c(\theta)}{T_c(0)} = 1 - R_\theta \theta^2 + O(\theta^4), \tag{1}$$

if the theory is analytic around $\theta = 0$.

A decreasing $T_c(\theta)$ means that the curvature R_θ is positive. A possible argument to understand such a decrease has been given in Ref. [11]. The free energy increases as a function of θ, and the coefficient of the lowest-order term, which is quadratic in θ, is given by $\chi/2$, where χ is the topological susceptibility [$\chi \equiv \langle Q^2 \rangle / (a^4 V)$ and $a^4 V$ is the spacetime volume]. Because of the sharp drop of χ across the deconfinement transition [20–22], the increase of free energy in the confined phase is larger than that in the deconfined phase; hence, as θ increases, it becomes more and more favorable to the system to stay in the deconfined phase, so that the deconfining temperature moves to lower temperatures. In particular, for a first-order transition, which is the case for SU(N) pure gauge theories with $N \geq 3$, one finds [11]

$$\frac{T_c(\theta)}{T_c(0)} = 1 - \frac{\Delta\chi}{2\Delta\epsilon}\theta^2 + O(\theta^4), \tag{2}$$

where $\Delta\epsilon$ and $\Delta\chi$ are, respectively, the jump of the energy density and the drop of the topological susceptibility at the transition. In the large-N limit, $\Delta\chi$ tends to χ computed at $T = 0$ and stays finite, while $\Delta\epsilon \propto N^2$, so that $R_\theta \propto 1/N^2$.

The first numerical results regarding R_θ have been given in Ref. [11] for the SU(3) pure gauge theory, exploiting the idea of performing simulations at imaginary values of θ in order to avoid the sign problem [7–10]. The approach is the same as that adopted for QCD at finite baryon chemical potential μ_B, where purely imaginary values of μ_B avoid complex values of the fermion determinant: one can then make use of analytic continuation to infer the dependence at real μ_B, at least for small values of μ_B/T [37]; in particular, the critical temperature can be reliably estimated up to the quadratic order in μ_B, while ambiguities related to the procedure of analytic continuation may affect higher-order terms [38]. The same approach can be used to explore physics at nonzero θ, if one assumes that the theory is analytic around $\theta = 0$, a fact supported by our present knowledge about free-energy derivatives at $\theta = 0$ [36,39–43].

In Ref. [11], the curvature R_θ was determined by analytic continuation on three different lattice sizes ($16^3 \times 4$, $24^3 \times 6$, and $32^3 \times 8$) corresponding to the same physical spatial volume and different lattice spacings [$a \simeq (4T_c)^{-1}$, $(6T_c)^{-1}$, and $(8T_c)^{-1}$, respectively] around the transition. This has allowed us to extrapolate the curvature to the continuum limit, obtaining $R_\theta = 0.0175(7)$, a value which is in rough agreement with the model prediction in Eq. (2) [11].

In the present study we make progress by performing new numerical simulations, both at zero and nonzero imaginary θ, on a $40^3 \times 10$ lattice. On the one hand, in Sec. II A we obtain a new determination of R_θ by analytic continuation on a finer lattice, which allows us to check and improve the continuum extrapolation of Ref. [11]. On the other hand, the determination of the topological background Q of configurations sampled at $\theta = 0$ will allow us to obtain direct information at real θ by reweighting techniques, as illustrated in Sec. II B: in this way we shall be able to check the reliability of analytic continuation and to put the numerical determination of R_θ on a more solid basis. Finally, Sec. II C is devoted to investigating the dependence of physical quantities, including the critical temperature, on the topological sector.

A. Results from imaginary θ

The partition function of lattice SU(N) gauge theories in presence of an imaginary theta term reads

$$Z_L(T, \theta_L) = \int [dU] e^{-S_L[U] - \theta_L Q_L[U]}, \tag{3}$$

where U stands for a configuration of gauge link variables, $U_\mu(n)$, while S_L and Q_L are the lattice discretizations of, respectively, the pure gauge action and the topological charge, $Q_L = \sum_x q_L(x)$. As in Ref. [11], we consider the Wilson plaquette action and a simple dicretization for q_L,

$$q_L(x) = \frac{-1}{2^9\pi^2} \sum_{\mu\nu\rho\sigma=\pm1}^{\pm4} \tilde{\epsilon}_{\mu\nu\rho\sigma} \mathrm{Tr}(\Pi_{\mu\nu}(x)\Pi_{\rho\sigma}(x)), \quad (4)$$

where $\Pi_{\mu\nu}$ is the plaquette operator, $\tilde{\epsilon}_{\mu\nu\rho\sigma} = \epsilon_{\mu\nu\rho\sigma}$ for positive directions, and $\tilde{\epsilon}_{\mu\nu\rho\sigma} = -\tilde{\epsilon}_{(-\mu)\nu\rho\sigma}$. With this choice, gauge links still appear linearly in the modified action, and hence a standard heat-bath algorithm over SU(2) subgroups, combined with over-relaxation, can be implemented; this would not be possible for different improved choices of q_L, like for instance smeared or fermionic operators.

In general, the lattice operator $q_L(x)$ is linked to the continuum $q(x)$ by a finite multiplicative renormalization [44],

$$q_L(x) \overset{a\to0}{\sim} a^4 Z(\beta) q(x) + O(a^6), \quad (5)$$

where $a = a(\beta)$ is the lattice spacing and $\lim_{a\to0} Z = 1$. Hence, as the continuum limit is approached, the imaginary part of θ is related to the lattice parameter θ_L appearing in Eq. (3) as follows: $\theta_I = Z\theta_L$.

Knowledge about $Z(\beta)$ is essential to fix the working physical value of θ_I. It is important to stress that other renormalizations, linked to the choice of the lattice operator q_L, may affect the free energy, e.g., in the form of additive renormalizations stemming from two (or more) point correlators of q_L. Such UV terms, however, are continuous across the phase transition, and hence they do not play a role in the determination of T_c as a function of θ_I: this is confirmed by the fact that, as shown in Ref. [11] and in the present paper, a consistent extrapolation to the continuum can be taken for R_θ.

Here we will make use of the nonperturbative determination of Z reported in Ref. [11]; see in particular Fig. 2 reported therein. This has been obtained by measuring, on symmetric $T = 0$ lattices, the following quantity [10]:

$$Z \equiv \frac{\langle Q Q_L \rangle}{\langle Q^2 \rangle}, \quad (6)$$

where Q is, configuration by configuration, the integer closest to the topological charge obtained after cooling [39,45]. The idea is similar to that used by heating techniques [46], where the average value of Q_L is determined within a fixed topological sector.

The new set of numerical simulations on the $40^3 \times 10$ lattice have been carried out at four different values of θ_L, $\theta_L = 0.0$, 6.0, 8.4 and 13.4. We have performed several series of simulations with a fixed θ_L and variable β. Typical statistics have been of $O(10^5)$ measurements per β at $\theta = 0$ and of $O(10^4)$ measurements per β at $\theta \neq 0$, each separated by an updating cycle of 4 over-relaxation $+1$ heat-bath sweeps. The somewhat larger statistics at $\theta = 0$ is justified in view of the further analysis reported in the following subsections. The numerical effort required for this new $N_t = 10$ lattice is significantly larger than that made in Ref. [11], both because of the larger lattice size and because of the larger autocorrelation times, going up to a few hundred cycles around the transition.

As in Ref. [11], in order to determine the deconfinement transition temperature, we have considered the Polyakov loop and its susceptibility,

$$L \equiv \frac{1}{V_s} \sum_{\vec{x}} \frac{1}{N} \mathrm{Tr} \prod_{t=1}^{N_t} U_0(\vec{x}, t), \quad \chi_L \equiv V_s(\langle |L|^2 \rangle - \langle |L| \rangle^2), \quad (7)$$

where V_s is the spatial volume and $|L|$ is the Polyakov loop modulus. Center symmetry, which corresponds to a multiplication of all parallel transports at a fixed time by an element of the center of the SU(N) gauge group, Z_N, is spontaneously broken at the deconfinement transition and the Polyakov loop—which is not invariant under center transformations—is a related order parameter. The modified action $S_L + \theta_L Q_L$ is also center symmetric, and hence the Polyakov is also an exact order parameter at $\theta \neq 0$.

The Polyakov loop susceptibility is plotted as a function of β in Fig. 1, together with data obtained after reweighting in β. As θ_L increases, the susceptibility peak moves to higher values of β, i.e., to higher temperatures $T = 1/(a(\beta)N_t)$.

The critical couplings $\beta_c(\theta_L)$ have been obtained by performing a Lorentzian fit to the un-reweighted data of the susceptibility. From $\beta_c(\theta_L)$ we reconstruct $T_c(\theta_L)/T_c(0) = a(\beta_c(0))/a(\beta_c(\theta_L))$ by means of the nonperturbative determination of $a(\beta)$ reported in Ref. [47]; in general, the location of T_c is affected by finite size corrections, which however should almost cancel when computing the

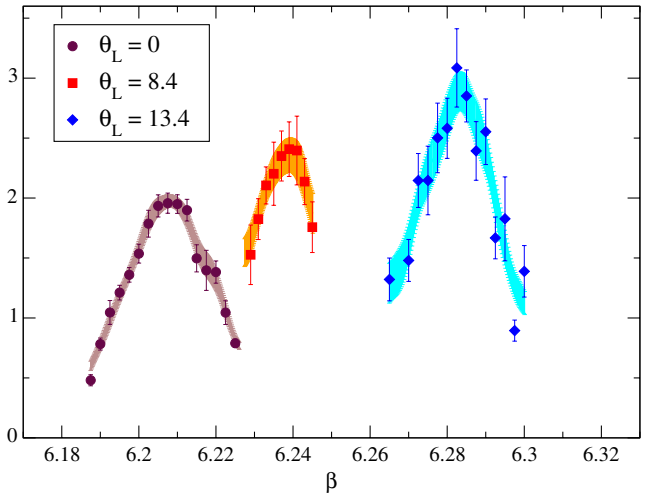

FIG. 1 (color online). Polyakov loop susceptibility as a function of β on the $40^3 \times 10$ lattice for some explored values of θ_L.

ratio $T_c(\theta_L)/T_c(0)$. Finally, θ_L must be converted into θ_I by exploiting the determination of Z at the critical coupling β_c, which is obtained by the interpolation of data reported in Ref. [11]. All results are shown in Table I, where we also report, for the reader's convenience, data obtained on different lattices in Ref. [11].

The values obtained for $T_c(\theta_I)/T_c(0)$ can be fitted according to Eq. (1), with $\theta_I^2 = -\theta^2$. If we restrict to $\theta_I < 2$, we get $R_\theta = 0.0200(5)$, with $\chi^2/\text{d.o.f.} \simeq 0.11$. As a final step, we can put the value of R_θ together with those obtained for smaller values of N_t in Ref. [11]; see Fig. 2. An extrapolation to the continuum limit assuming $\mathcal{O}(a^2)$ corrections, $R_\theta(N_t) = R_\theta^{\text{cont}} + b/N_t^2$, yields $R_\theta^{\text{cont}} = 0.0178(5)$, with $\chi^2/\text{d.o.f.} \simeq 0.6$. This is consistent with the continuum extrapolation reported in Ref. [11], and in rough agreement with the leading $1/N$ estimate for SU(3), $R_\theta = 0.028(6)$ [11]. The most significant correction to the large-N prediction can be attributed to the fact that, for finite N, the susceptibility does not drop sharply to zero at the transition, i.e., $\Delta\chi$ in Eq. (2) is less than the value of χ in the confined phase.

B. Comparison with reweighting at real θ

Presently known solutions to the sign problem are only approximate and typically introduce assumptions and systematic errors. In the case of analytic continuation an obvious assumption is that of analyticity around $\theta = 0$.

TABLE I. Collection of results obtained for β_c and T_c. Results for $N_t = 4$, 6, 8 are taken from Ref. [11] and reported for completeness.

Lattice	θ_L	β_c	θ_I	$T_c(\theta_I)/T_c(0)$
$16^3 \times 4$	0	5.6911(4)	0	1
$16^3 \times 4$	5	5.6934(6)	0.370(10)	1.0049(11)
$16^3 \times 4$	10	5.6990(7)	0.747(15)	1.0171(12)
$16^3 \times 4$	15	5.7092(7)	1.141(20)	1.0395(11)
$16^3 \times 4$	20	5.7248(6)	1.566(30)	1.0746(10)
$16^3 \times 4$	25	5.7447(7)	2.035(30)	1.1209(10)
$24^3 \times 6$	0	5.8929(8)	0	1
$24^3 \times 6$	5	5.8985(10)	0.5705(60)	1.0105(24)
$24^3 \times 6$	10	5.9105(5)	1.168(12)	1.0335(18)
$24^3 \times 6$	15	5.9364(8)	1.836(18)	1.0834(23)
$24^3 \times 6$	20	5.9717(8)	2.600(24)	1.1534(24)
$32^3 \times 8$	0	6.0622(6)	0	1
$32^3 \times 8$	5	6.0684(3)	0.753(8)	1.0100(11)
$32^3 \times 8$	8	6.0813(6)	1.224(15)	1.0312(14)
$32^3 \times 8$	10	6.0935(11)	1.551(20)	1.0515(21)
$32^3 \times 8$	12	6.1059(21)	1.890(24)	1.0719(34)
$32^3 \times 8$	15	6.1332(7)	2.437(30)	1.1201(17)
$40^3 \times 10$	0	6.2082(4)	0	1
$40^3 \times 10$	6	6.2236(8)	1.068(7)	1.0232(14)
$40^3 \times 10$	8.4	6.2381(5)	1.509(10)	1.0453(10)
$40^3 \times 10$	13.4	6.2821(9)	2.461(22)	1.1144(16)

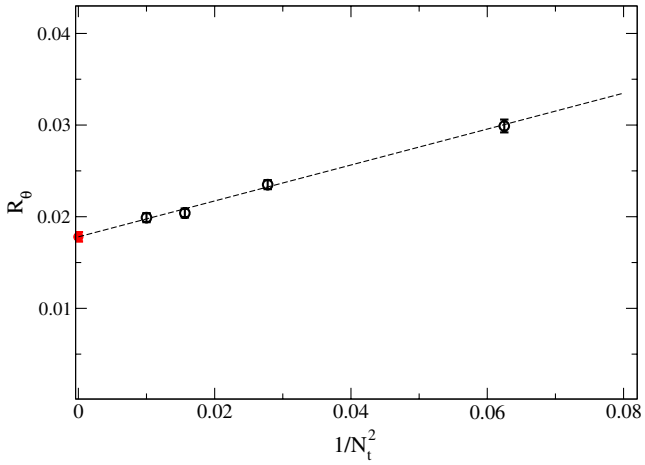

FIG. 2 (color online). R_θ as a function of $1/N_t^2$. The point at $1/N_t = 0$ is the continuum limit extrapolation, assuming $\mathcal{O}(a^2)$ corrections.

A possible way to keep such effects under control is to compare different, independent methods, thus cross-checking results.

An alternative method to analytic continuation, which has been largely used in QCD at finite baryon chemical potential, is reweighting. The idea is to sample configurations at $\theta = 0$ and to move the complex factor of the path integral measure into the observable, i.e., for a generic quantity O,

$$\langle O \rangle_\theta = \frac{\int [dU] e^{-S_L[U] + i\theta Q} O}{\int [dU] e^{-S_L[U] + i\theta Q}} = \frac{\langle e^{i\theta Q} O \rangle}{\langle \cos(\theta Q) \rangle}, \qquad (8)$$

where averages without a subscript are taken as usual at $\theta = 0$, and the equality $\langle e^{i\theta Q} \rangle = \langle \cos(\theta Q) \rangle$ has been used, which derives from the symmetry under $Q \to -Q$ of the distribution at $\theta = 0$. The major drawback of reweighting is that configurations sampled at $\theta = 0$ may not be representative enough of the physics at $\theta \neq 0$; such a problem gets worse and worse as θ increases and as the thermodynamical limit is approached. A measure of the severeness of the problem is given by the average phase factor in the denominator of Eq. (8): as $\langle \cos(\theta Q) \rangle$ vanishes, one would need unfeasibly large statistics to keep statistical errors under control. Such problems are well known from QCD at finite baryon density [48]: a partial improvement can be achieved by reweighting in more than one parameter [49].

Since in the reweighting method the topological charge does not enter the sampling algorithm directly, one can make use of smoothed gluonic or fermionic definitions of Q in order to avoid issues related to renormalization. However, the implementation must be cheap enough to permit the collection of a sufficiently large sample of measures. We have adopted cooling, in particular the implementation outlined in Ref. [39], which is known to provide reliable results on fine enough lattices. This is the reason why we have decided to apply the reweighting

method only to configurations sampled on the $N_t = 10$ lattice. Q has been measured once every four updating cycles; we will show results for Q obtained after $n_{\rm cool} = 30$ cooling sweeps; however, we have checked that different choices lead to compatible results.

Let us start the discussion of our results by showing, in Fig. 3, the behavior of the average phase factor $\langle \cos(\theta Q)\rangle$ as a function of θ for three different bare couplings, $\beta = 6.1600$, 6.2075, and 6.2475, corresponding to $T \simeq 0.93T_c$, T_c, and $1.06T_c$, respectively. In Fig. 4 we also show $\langle \cos(\theta Q)\rangle$ as a function of $n_{\rm cool}$ for a few values of θ at $T \simeq 1.06T_c$, which nicely demonstrates the stability of results under different choices of $n_{\rm cool}$.

The regions where $\langle \cos(\theta Q)\rangle$ becomes very small are hardly accessible to reweighting. It is clear that the situation is worse in the confined phase, where only $\theta \lesssim 0.2\pi$ seems accessible, than in the deconfined phase where $\theta \sim 0.5\pi$ seems reachable. This can be understood in terms of the much lower topological activity present in the deconfined phase. It should be stressed, however, that as the thermodynamical limit $V_s \to \infty$ is taken, arbitrarily large fluctuations of the global charge Q are expected in both phases, so that $\langle \cos(\theta Q)\rangle$ must drop to zero for any $\theta \neq 0$.

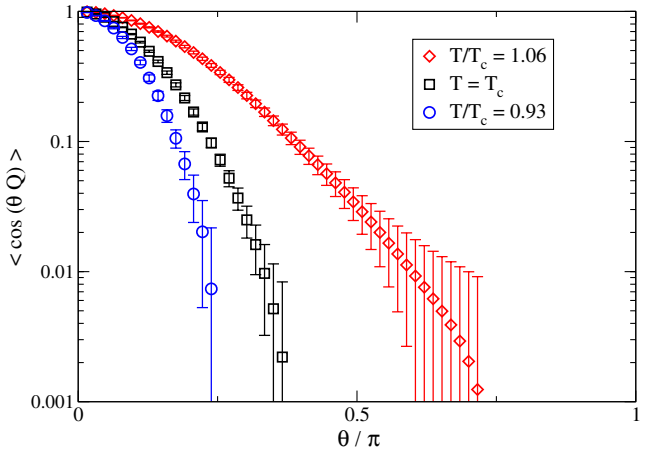

FIG. 3 (color online). Dependence of $\langle \cos(\theta Q)\rangle$ on θ on the $40^3 \times 10$ lattice and for three different values of T.

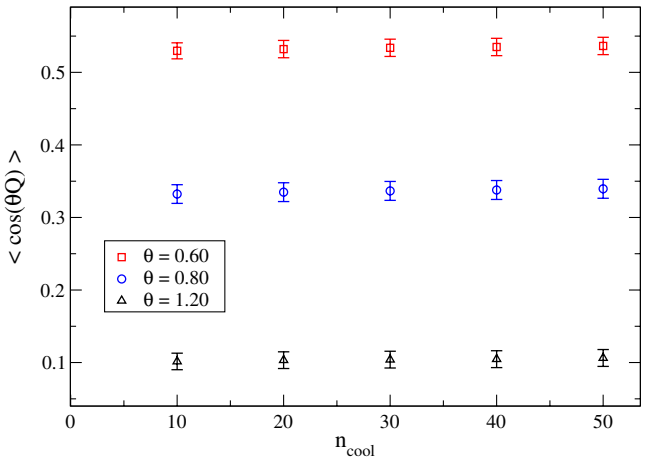

FIG. 4 (color online). Dependence of $\langle \cos(\theta Q)\rangle$ on the number of cooling steps for $T \simeq 1.06T_c$ and three values of θ.

Let us now discuss the behavior of physical quantities computed at nonzero θ via reweighting, and compare it with results obtained at imaginary θ. We are interested, in particular, in the Polyakov loop modulus,

$$\langle |L| \rangle_\theta = \frac{\langle e^{i\theta Q}|L|\rangle}{\langle e^{i\theta Q}\rangle} = \frac{\langle \cos(\theta Q)|L|\rangle}{\langle \cos(\theta Q)\rangle}, \tag{9}$$

and in its susceptibility, $\chi_L(\theta) = V_s(\langle |L|^2\rangle_\theta - \langle |L|\rangle_\theta^2)$. The ratio of expectation values in Eq. (9) is computed via a jackknife algorithm. We have also replaced $e^{i\theta Q}$ with $\cos(\theta Q)$ in the numerator, since L, as well as the path integral measure at $\theta = 0$, is invariant under parity transformations, under which instead $Q \to -Q$.

In Fig. 5 we show the dependence of the Polyakov loop on θ^2 for a selected value of the bare coupling, $\beta = 6.245$, corresponding to $T \sim 1.055T_c$. Results at $\theta^2 \leq 0$ derive from direct simulations, while those at $\theta^2 > 0$ have been obtained via reweighting from $\theta = 0$ data. All data can be nicely fitted by a linear dependence in θ^2, as shown in the figure, demonstrating that analyticity around $\theta = 0$ holds within errors. The range of explored θ^2 values is limited on the right by the feasibility of reweighting, while on the left one must avoid the crossing of the deconfining transition, which moves to higher values of T as θ^2 decreases (see Fig. 7).

The increasing behavior of $\langle |L| \rangle$ can be understood by considering that one moves deeper and deeper into the deconfined phase as θ^2 increases: the quadratic behavior in θ^2 is consistent with analyticity around $\theta^2 = 0$ and with

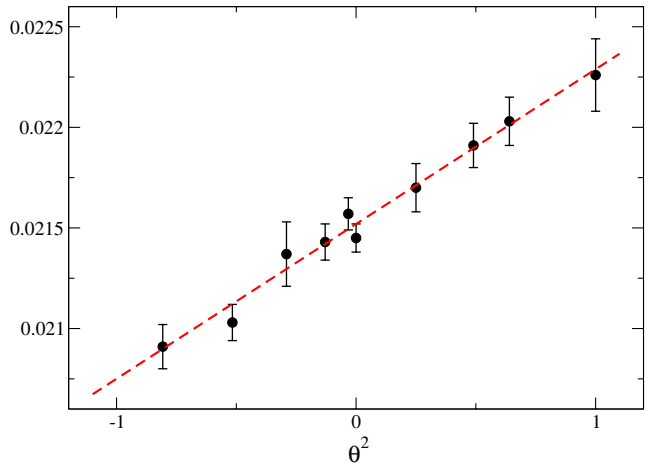

FIG. 5 (color online). Dependence of the Polyakov loop modulus on θ^2 for $T \simeq 1.055T_c$ on the $40^3 \times 10$ lattice. The dashed line is a best fit according to a linear dependence on θ^2.

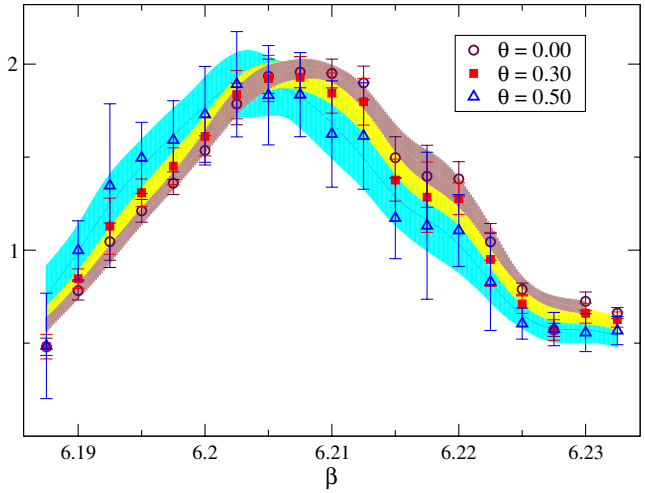

FIG. 6 (color online). Polyakov loop susceptibility as a function of β and after reweighting at a few values of real θ. The shaded bands correspond to data that are also reweighted in β.

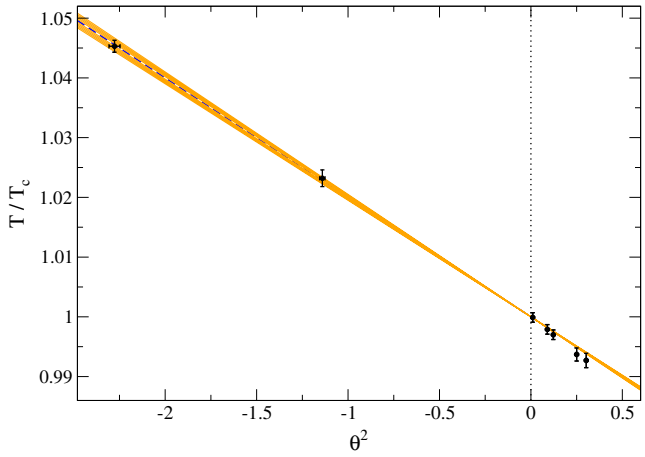

FIG. 7 (color online). Critical temperature as a function of θ^2: we report the result of the linear fit in θ^2 obtained from simulations at $\theta^2 < 0$.

the fact that $\langle |L| \rangle$ is a P-even quantity. We notice that both features are consistent with the results of Ref. [15].

Finally, in Fig. 6 we show results for the susceptibility as a function of β, obtained after reweighting at $\theta = 0.3$ and 0.5, together with the original data at $\theta = 0$. It is clear that the peak moves to lower values of β, i.e., to lower temperatures, as θ increases, in agreement with results from analytic continuation. From the susceptibility peaks we can extract the critical temperatures (see Table II), and compare them with results at imaginary θ. It does not make sense to fit reweighted data directly, since they are obtained from the same data sample and are therefore correlated; instead, in Fig. 7 we compare reweighted data with the extrapolation linear in θ^2 obtained by fitting results at imaginary θ, showing that there is indeed agreement, within statistical errors.[1] This gives further support to the validity of analytic continuation, at least for small values of θ.

TABLE II. Results obtained for β_c and T_c at real θ by the reweighting technique on the $40^3 \times 10$ lattice. The ratios of critical temperatures have been calculated using the $\theta = 0$ critical β reported in Table I.

Lattice	θ	β_c	$T_c(\theta)/T_c$
$40^3 \times 10$	0.10	6.2081(4)	0.9999(8)
$40^3 \times 10$	0.30	6.2068(4)	0.9979(8)
$40^3 \times 10$	0.35	6.2062(5)	0.9970(8)
$40^3 \times 10$	0.50	6.2040(6)	0.9937(11)
$40^3 \times 10$	0.55	6.2033(7)	0.9927(12)

C. Deconfinement and the Polyakov loop at fixed topological background

The general expression for a reweighted observable, Eq. (8), can be rewritten in the following form:

$$\langle O \rangle_\theta = \frac{1}{\langle \cos(\theta Q) \rangle} \sum_{Q=-\infty}^{\infty} e^{i\theta Q} \mathcal{P}(Q) \langle O \rangle_Q, \qquad (10)$$

where $\langle \cdot \rangle_Q$ stands for the average in a given topological sector and $\mathcal{P}(Q)$ is the topological charge distribution at $\theta = 0$. It shows that a nontrivial dependence on θ is possible only if the observable has a nontrivial dependence on Q. This is quite natural, since θ and Q are conjugate quantities, like the particle density and the chemical potential.

The fact that, as we have shown, the location of deconfinement moves as θ is changed, leads us to suspect that the dependence of physical observables on Q may be significant around T_c. Investigating such a dependence is quite important for various reasons, for instance to understand the possible systematic effects involved in numerical simulations carried out in a fixed topological sector, as it happens when investigating QCD with overlap fermions. Studies regarding such effects have been reported, both at zero and finite T [23–25]; in particular, a recent study has shown that systematic effects in the determination of the topological susceptibility at finite T are well under control [25]. In the present subsection we will discuss the dependence on Q of quantities directly related to deconfinement, in particular the Polyakov loop and its susceptibility, showing

[1] If one wants to extract the curvature from reweighting, taking into account that results at different real values of θ are strongly correlated, then a reasonable estimate is obtained by considering only the point at the largest feasible value of θ, i.e., $\theta = 0.55$. This yields—assuming that such a value is in the linear region, i.e., that $R_\theta \simeq (1 - T_c(\theta)/T_c(0))/\theta^2$—the value $R_\theta = 0.024(4)$, in agreement with the estimate from analytic continuation for $N_t = 10$, $R_\theta = 0.0200(5)$.

that in this case systematic effects, even if disappearing in the thermodynamical limit, can be more significant.

Such a study is best performed on the finest lattice at our disposal, i.e., the $40^3 \times 10$, where the determination of the topological background is most reliable. For that reason we have divided the set of configurations sampled at each β according to the value of Q obtained via cooling, as discussed in the previous subsection. The expectation value $\langle\cdot\rangle_Q$ is obviously independent of θ since, in a fixed topological background, θ only adds an irrelevant overall phase factor, and hence in principle one may think of combining equal Q configurations sampled at different imaginary values of θ. However, one must consider that the lattice charge operator entering Eq. (3) contains irrelevant discretization terms, which are not constant over a given topological sector and may lead to a residual dependence on θ_L. For this reason, in the following we will consider only configurations sampled at $\theta = 0$.

Let us start by showing, in Fig. 8, the behavior of the Polyakov loop as a function of Q for a few temperatures around T_c,

$$\langle |L| \rangle_{|Q|} = \frac{\sum_{i=1}^{N} |L|_i \delta_{|Q|,|Q_i|}}{\sum_{i=1}^{N} \delta_{|Q|,|Q_i|}}, \tag{11}$$

where i runs over the N measures and we have combined measures from opposite topological sectors, exploiting the symmetry of the Polyakov loop under parity transformations, in order to reduce statistical errors. The exact symmetry visible in Fig. 8 is therefore artificial; however, we have verified that the symmetry holds, within errors, even before such a combination. We observe that, while below the transition the dependence on $|Q|$ is quite mild, it gets stronger at the transition and becomes only slightly milder above T_c. A similar behavior is observed for the average plaquette, even if in this case the relative variation from

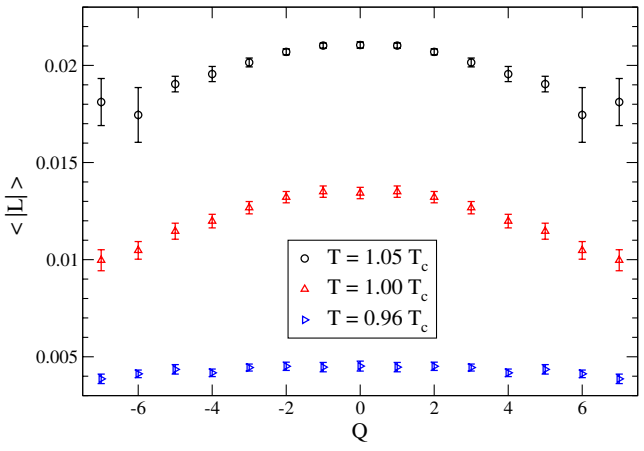

FIG. 8 (color online). Dependence of the Polyakov loop modulus on the topological sector Q, determined on the $40^3 \times 10$ lattice and for a few values of T around the transition.

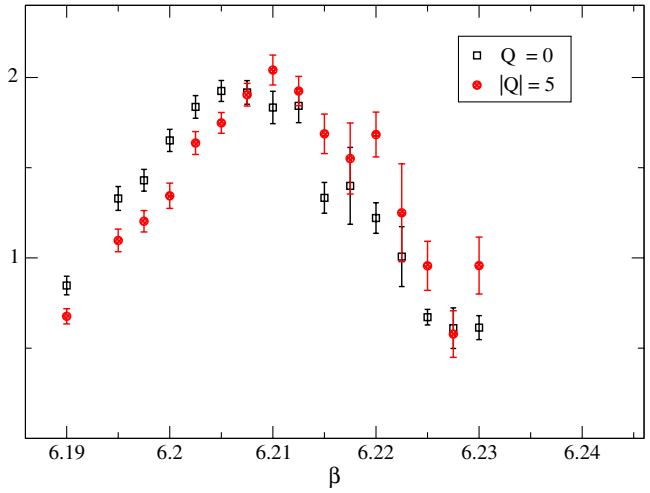

FIG. 9 (color online). Susceptibility of the Polyakov loop as a function of β on the $40^3 \times 10$ lattice, determined after fixing the topological sector.

one sector to the other is always modest and never larger than 10^{-4}.

The dependence on Q is also quite visible in the susceptibility of the Polyakov loop, which is shown in Fig. 9 as a function of β for $Q = 0$ and $|Q| = 5$. The shift of the susceptibility peaks tells us that even the transition temperature can be influenced by the overall topological background. In particular, in Table III, we report the values of $T_c(Q)$, obtained by fitting such peaks with Lorentzian functions. The critical temperature tends to increase as $|Q|$ increases; this is qualitatively consistent with that found when adding an imaginary θ term, which has the effect of shifting the average value of the topological charge distribution towards nonzero values.

One expects that systematic effects present in a fixed sector Q disappear as the thermodynamical limit is approached. In order to verify this, we have performed—for a given value of $T \simeq 1.018 T_c$ ($\beta = 6.22$)—simulations on lattices with different spatial volumes ($L_s^3 \times L_t$ with $L_t = 10$ and $L_s = 16, 18, 20, 25, 30, 35, 40$), and then combined measures obtained within different topological sectors Q as described above. In Fig. 10 we show how the difference of the Polyakov loop modulus in the $Q = 0$ sector, taken

TABLE III. Results obtained for β_c and T_c at fixed topology calculated with $\beta_c = 6.2082(4)$.

Lattice	$\lvert Q\rvert$	β_c	$T_c(Q)/T_c$
$40^3 \times 10$	0	6.2065(5)	0.9975(10)
$40^3 \times 10$	1	6.2068(5)	0.9978(10)
$40^3 \times 10$	2	6.2069(5)	0.9981(10)
$40^3 \times 10$	3	6.2080(5)	1.0000(10)
$40^3 \times 10$	4	6.2092(5)	1.0015(10)
$40^3 \times 10$	5	6.2108(7)	1.0039(12)
$40^3 \times 10$	6	6.2118(7)	1.0053(12)

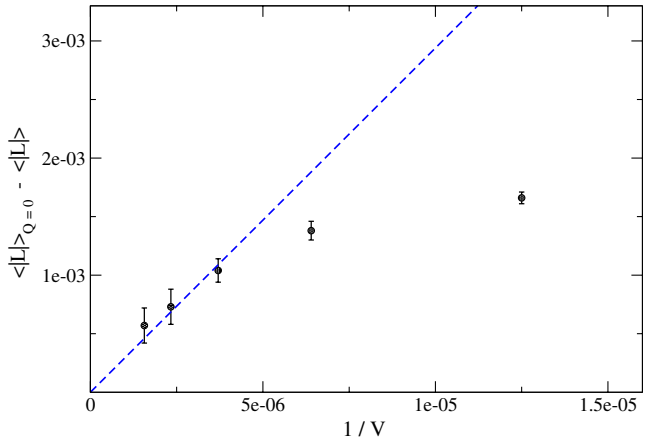

FIG. 10 (color online). Variation of the Polyakov loop modulus in the $Q = 0$ sector, with respect to the average over all sectors, plotted as a function of $1/V$, for $T \simeq 1.018 T_c$. The dashed line is the result of a linear fit in $1/V$.

with respect to its average over all sectors, changes as a function of the volume $V = L_t L_s^3$. The difference clearly approaches zero linearly in $1/V$, as one indeed expects on general grounds.

We will now try to better describe the observed dependence of the Polyakov loop on Q by a very simplified model, which is based on the instanton gas approximation and follows the analysis reported in Ref. [23]. Let us consider a generic, extensive quantity, like the average Polyakov loop times the volume V: we assume that it receives a given, fixed contribution from each topological object—instanton or anti-instanton—and that the topological objects are distributed according to the instanton gas approximation, i.e., that the probability of having n instantons and $\bar{n}$ anti-instantons is given by

$$\mathcal{P}(n, \bar{n}) = e^{-2\lambda} \frac{\lambda^n \lambda^{\bar{n}}}{n! \bar{n}!}, \tag{12}$$

where $2\lambda = \langle Q^2 \rangle = V \chi_l$ and $\chi_l = a^4 \chi$. The relevant quantity to describe the behavior as a function of $Q = n - \bar{n}$ is the average of the total number of topological objects which are found at fixed Q, $\langle n + \bar{n} \rangle_Q$, which can be extracted as a constrained average starting from the double Poisson distribution in Eq. (12). The result obtained at the lowest order in $Q^2/(2\lambda) = Q^2/\langle Q^2 \rangle$, which is the relevant expansion parameter when approaching the thermodynamical limit, is [23]

$$\langle n + \bar{n} \rangle_Q \simeq 2\lambda - \frac{1}{2}\left(1 - \frac{Q^2}{2\lambda}\right). \tag{13}$$

The prediction for $\langle |L| \rangle_Q$, which follows from our simplified model, is then

$$\langle |L| \rangle_Q = \text{const} - \frac{\gamma}{V} \langle n + \bar{n} \rangle_Q \simeq \langle |L| \rangle + \frac{\gamma}{2V}\left(1 - \frac{Q^2}{V \chi_l}\right), \tag{14}$$

where we have defined $-\gamma$ as the contribution to $V|L|$ coming from each (anti-)instanton and we have exploited the fact that the expression in parentheses vanishes when taking the average over all sectors.

Equation (14), which is expected to be valid as the thermodynamical limit is approached, predicts that $\langle |L| \rangle_Q - \langle |L| \rangle$ will vanish linearly in $1/V$. This is confirmed by the behavior shown in Fig. 10, and a linear fit to data on the larger volumes, which is shown in the same figure, gives $\gamma \sim 6 \times 10^2$. It is interesting that, once γ is fixed and since we know from the average over the whole ensemble that $\chi_l = \langle Q^2 \rangle / V \sim 0.947 \times 10^{-5}$, the behavior of the Polyakov loop as a function of Q in the large-volume limit is completely fixed by the model, in particular $\langle |L| \rangle_{Q=0} - \langle |L| \rangle_{|Q|} \simeq \gamma Q^2/(2\chi V^2)$. In order to check this, in Fig. 11 we plot the quantity

$$\Sigma(|Q|) = \frac{\langle |L| \rangle_{Q=0} - \langle |L| \rangle_{|Q|}}{\langle |L| \rangle_{Q=0}}, \tag{15}$$

which gives the relative deviation of the Polyakov loop from the value it takes in the trivial topological sector [the error on $\Sigma(|Q|)$ has been obtained by a jackknife algorithm]. In particular, we plot $\Sigma(|Q|)$ as a function of $|Q|/V$ for $|Q| = 1, 2, 3$ and for all the explored volumes, together with the model prediction, which has no more free parameters left. The fair agreement observed for small values of $|Q|/V$ is therefore highly nontrivial, given the crudeness of the model: part of the success can be ascribed to the rapid approach to the instanton gas approximation which takes place right above T_c, as demonstrated by the results of Ref. [36]. As $|Q|/V$ increases, however, the topological background is not dilute enough and the model prediction fails.

It would be nice to study the interplay between topological activity and the holonomy in more detail, in

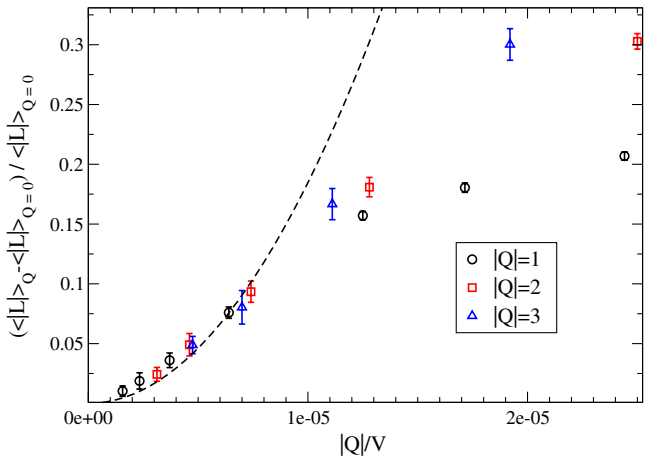

FIG. 11 (color online). Relative variation of the Polyakov loop modulus with the topological background, plotted as a function of the topological charge density $\frac{Q}{V}$, for $T \simeq 1.018 T_c$. Results have been obtained on different spatial volumes, the dashed line is the prediction from the simple model described in the text.

particular approaching the deconfining transition from above, and to compare with model studies regarding the same issue (see, e.g., Ref. [50]); however, this goes beyond the purpose of our present investigation.

Finally, it is important to stress that—despite the fact that the approach to the thermodynamical limit of $\langle |L| \rangle_Q$ seems to be well understood and that systematic effects vanish as $1/V$—from Fig. 11 we learn that they are still appreciable, and of the order of 10%, even on the largest explored volume, whose aspect ratio $L_s/L_t = 4$ is common to many finite-temperature computations found in the literature.

III. PHASE DIAGRAM IN THE T-θ PLANE: GENERAL FEATURES AND ANALOGIES WITH THE DIAGRAM AT IMAGINARY μ_B

After studying $T_c(\theta)$, it is tempting to draw a sketch of the whole phase diagram in the T-θ plane. On the imaginary side, $\theta = i\theta_I$, no particular structure is expected *a priori*, since CP symmetry is explicitly broken whenever $\mathrm{Im}(\theta) \neq 0$. Indeed, we have not observed any transition, apart from the deconfining one, in the range of explored values of θ_I, even if we cannot exclude the presence of new phase structures at larger values of θ_I.

The situation is quite different for real θ, which plays the role of an angular variable. The periodicity in θ must be reflected in some way in the structure of the phase diagram in the T-θ plane, which is then expected to be nontrivial. It is interesting to notice that this is very similar to what happens in the presence of an imaginary baryon chemical potential μ_B, and indeed many analogies can be found between the T-θ phase diagram and the phase structure at imaginary μ_B [11,17–19,51]. It is convenient, for the following discussion, to introduce the parameter $\theta_B \equiv \mathrm{Im}(\mu_B)/T$, since it allows analogies to appear more clearly.

The purpose of the present section is to discuss such analogies—also in a large-N perspective—with a particular emphasis on duality, in the sense of an inversion between the high- and low-temperature regions, between the T-θ and T-θ_B phase diagrams, which can be suggestive of the possible dual role played by the respective relevant degrees of freedom.

We will start by giving a rapid overview of the T-θ_B phase diagram in order to highlight aspects which may have a direct correspondence with the case of the T-θ plane, which is discussed afterwards.

A. Phase diagram in the T-θ_B plane

Let us consider QCD with N colors and its partition function at nonzero baryon chemical potential,

$$Z(T, \mu_B) = \mathrm{Tr} \exp\left(-\frac{H - \mu_B B}{T}\right), \tag{16}$$

where H is the QCD Hamiltonian and B is the baryon number operator. For purely imaginary values of μ_B, which are often considered to avoid the sign problem, the partition function becomes

$$Z(T, \theta_B) = \mathrm{Tr}(e^{-\frac{H}{T}} e^{i\theta_B B}), \tag{17}$$

where $\theta_B = \mathrm{Im}(\mu_B)/T$.

It is clear that θ_B plays the role of an angular variable; however, the actual dependence of the free energy on θ_B depends on the phase of the theory. In the confined phase, θ_B couples only to physical degrees of freedom which have integer baryon charge B, and hence the free energy is a function of θ_B with period 2π. Instead, in the deconfined phase, new physical degrees of freedom appear, quarks, carrying a fractional baryon charge, in particular in units of $1/N$: as a consequence the free energy is expected to be a function of θ_B/N.

One may expect then that the periodicity in θ_B is $2\pi N$, but instead it is easy to prove that, independently of the relevant degrees of freedom, the partition function must be periodic in θ_B with period 2π. Indeed, in the path integral representation of the partition function

$$Z = \int \mathcal{D}A e^{-S_G[A]} \det M[A], \tag{18}$$

where $\det M[A]$ is the quark determinant, the imaginary chemical potential enters as a twist, by a phase factor $\exp(i\theta_B/N)$, in the boundary conditions for quark fields. However, for $\theta_B = 2\pi k$ with k an integer, such a twist can be cancelled exactly by a center transformation on the gauge fields, i.e., by a gauge transformation periodic in time up to a global element of Z_N, the center of the gauge group, $\exp(i2\pi k/N)$, under which the pure gauge action is invariant. As a consequence, the partition function and the free energy must be always periodic in θ_B, with period 2π.

How is it possible to reconcile such periodicity with the expected dependence on θ_B/N in the deconfined phase? This is done by a nonanalytic, multibranched behavior of the free energy, as a function of θ_B, in the high-temperature deconfined phase, with phase transitions happening at $\theta_B^{(\mathrm{RW})} = (2n + 1)\pi$ (n being a relative integer) which are known as Roberge-Weiss (RW) transitions [52]. When crossing such values, gauge fields jump discontinuously from one center sector to the other, characterized by a different global alignment of the Polyakov loop. One has, therefore, N different branches, which are not equivalent from the point of view of the order parameter $\langle L \rangle$ but whose free energies are identical, modulo a shift $\theta_B \to \theta_B + 2\pi$, by virtue of the invariance of the pure gauge action under center transformations.

Let us try to better clarify the role played by the center symmetry. Z_N is broken explicitly by the presence of the quark determinant; however, a residual Z_2 symmetry exists for particular values of θ_B, $\theta_B = k\pi$, with k a relative integer. Such residual symmetry can be identified, modulo a phase rotation, with charge conjugation C. It stays always unbroken for even values of k; on the other hand, it breaks spontaneously, in the high-T phase, for odd values of k, for

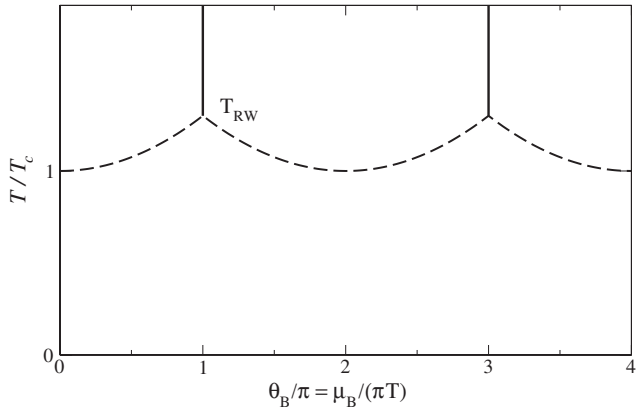

FIG. 12. Phase diagram of QCD in the presence of an imaginary baryon chemical potential μ_B as it emerges from symmetry considerations and numerical simulations. The vertical lines are the Roberge-Weiss transition lines present in the high-T phase of the theory, the dashed lines represent the deconfining transition, and T_{RW} indicates the temperature at which the Roberge-Weiss lines terminate (see text).

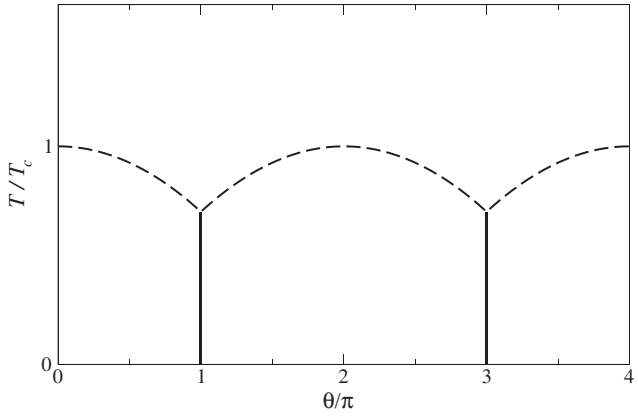

FIG. 13. Conjectured phase diagram of the pure gauge SU(N) Yang-Mills theories in the T-θ plane. The vertical lines are the first-order transition lines expected in the low-T phase of the theory, and the dashed lines correspond to the deconfining transition.

which the effective potential of the Polyakov loop has two equivalent, degenerate minima, corresponding to adjacent center sectors [52].

The RW transitions and their connection with the deconfining, chiral restoring (pseudo)critical line $T_c(\theta_B)$ have been widely studied both by numerical lattice simulations and by effective model computations [53–68]. The resulting diagram in the T-θ_B plane is sketched in Fig. 12.

The RW transition lines are first order and correspond to a discontinuous jump in the order parameter, the Polyakov loop. The order of their end point, however, depends on the quark mass spectrum: evidence from lattice studies collected up to now is that, for both the two-flavor and the three-flavor theory, the end point is second order for intermediate quark masses and first order in the limit of large or small quark masses [54–56]. In the former case the universality class is that of the three-dimensional Ising model, since the relevant symmetry is Z_2; in the latter, the end point is actually a triple point, with two further first-order lines departing from it, which can be identified with part of the (pseudo)critical lines $T_c(\theta_B)$ corresponding to chiral symmetry restoration and deconfinement. The line $T_c(\theta_B)$ is therefore a multibranched function itself, with cusps which can be conjectured to coincide with the RW end points, as depicted in Fig. 12: this is also consistent with available numerical evidence.

B. Phase diagram in the T-θ plane

In presence of a real θ term, gauge configurations are weighted in the path integral representation of the partition function by a factor $\exp(i\theta Q)$. The topological charge Q is globally an integer for finite-action configurations, and hence the partition function and the free energy must be periodic in θ, with period 2π.

However, if one searches for a θ dependence which stays nonzero at the leading order in $1/N$, as required by the solution to the axial U(1) problem, one needs the free energy to be a function of θ/N, instead of θ, because otherwise the θ dependence would be suppressed exponentially in N [1].

Also in this case, the only possible way to reconcile periodicity in θ and dependence on θ/N is to admit that the free-energy density $f(\theta)$ is a multibranched function of θ [26–28], scaling in the large-N limit as follows [26,28]:

$$f(\theta) = N^2 \min_k h\left(\frac{\theta + 2\pi k}{N}\right), \tag{19}$$

where k runs over all relative integers. For each value of θ the system chooses the branch that minimizes the free energy. The function h can be chosen so as to have its minimum at zero [69], so that the branch relevant to $\theta \sim 0$ corresponds to $k = 0$. Moreover, the invariance under CP, present at $\theta = 0$, imposes that h is an even function of θ.

A shift $\theta \to \theta + 2\pi$ corresponds to a passage from one branch to the other, which, according to the large-N scaling in Eq. (19), must happen discontinuously at points where the free energies of the two adjacent branches cross with different (opposite) derivatives, i.e., through a first-order transition. For symmetry reasons this happens for $\theta = \pm\pi$, or odd multiples of such values. CP symmetry, which is exact in correspondence of such points, is broken spontaneously by the choice of one of the two equivalent branches, which are not invariant under CP but are instead exchanged into each other. CP is of course also exact for $\theta = 0$ and for integer multiples of 2π, but there no spontaneous breaking happens.

The scenario depicted above is true only for sufficiently low temperatures. Indeed, in the opposite limit of high T, the instanton gas approximation must set in, which predicts

a smooth, periodic behavior in θ, but with an exponential suppression in the limit of large N [3,4].[2]

Actually, it has been conjectured [29–35] and recently proven by lattice simulations [36] that the change in θ dependence happens exactly in correspondence with the deconfinement transition. Therefore, while the confined phase is characterized by a dependence on θ/N and a nonanalytic periodicity in θ induced by the multibranched structure of the free energy, the deconfined phase is characterized by a smooth, periodic dependence on θ which is suppressed like e^{-N} in the large-N limit and rapidly approaches the instanton gas prediction[3]: in this case, of course, no CP breaking transition is expected at $\theta = \pi$. Hence, the CP-breaking transition lines, present for $\theta^{(CP)} = (2n+1)\pi$ and for low enough temperatures, must end at some temperature around T_c: as for the case of the RW lines, since the relevant symmetry is again Z_2, their end point can be either first order or second order in the three-dimensional Ising universality class.

The scenario described above is reproduced in Fig. 13, where we have drawn a sketch of the T-θ phase diagram. We have not made any discussion yet regarding the deconfinement line $T_c(\theta)$, but let us stop for while to comment on the analogy with the periodic structure in the T-θ_B plane, which now appears quite clearly. The analogy actually implies an exchange between the high-T and low-T regions of the two diagrams, i.e., $T \to 1/T$, which is suggestive of the possible dual role played by the relevant degrees of freedom in the two cases.

We have already discussed how the analytic or nonanalytic periodic structure of the T-θ_B plane can be understood in terms of a dependence of the free energy on θ_B (low T) or θ_B/N (high T), which in turn stems from the relevant degrees of freedom being hadrons with integer baryon charge B, or quarks carrying fractional baryon charge in units of $1/N$. If one wants to apply a similar, intuitive picture to the T -θ plane, one has to conjecture that the relevant topological degrees of freedom carry integer values of Q in the high-T, deconfined phase (in agreement with the instanton gas picture), but carry fractional charges, in units of $1/N$, in the low-T, confined phase.

Actually, such a hypothesis is not new. Indeed, the possible existence of topological objects with fractional charge—which are sometimes called instanton quarks—and their possible role in the confined phase have been conjectured in the past [33–35,70–80]. In the high-T, deconfined phase, they are expected to be localized and confined into larger objects carrying integer topological charge, like instantons and calorons. However, in the low-T, confined phase, they are expected to be free and delocalized topological objects.

Apart from the CP-breaking lines, the conjectured diagram sketched in Fig. 13 is completed by the deconfinement line $T_c(\theta)$, which we have discussed for SU(3) and small values of θ in the previous section. It is reasonable to assume—also based on the large-N model of Ref. [11]—that $T_c(\theta)$ is fixed by the interplay between thermodynamics and topological properties of the theory: since topology is exponentially suppressed in the deconfined phase, the leading dependence of $T_c(\theta)$ must derive from the topological properties of the confined phase, and hence we expect [11] that $T_c(\theta)$ will also be a multibranched function of θ/N, dominated, at the leading order in $1/N$, by the quadratic term

$$T_c(\theta)/T_c(0) \simeq 1 - R_\theta \min_k (\theta + 2\pi k)^2, \qquad (20)$$

where k is a relative integer and R_θ is $O(1/N^2)$.

Therefore, our expectation is that, at least for large enough N, the deconfinement temperature tends to a finite, nonzero value at $\theta = \pi$ or odd multiples of it (actually, θ independence is expected as $N \to \infty$). The periodicity in θ implies the presence of cusps for $T_c(\theta)$ at $\theta = (2k+1)\pi$. Notice that the phase structure may be more complicated in the presence of dynamical fermions, which have not been considered in this context: one can still predict the presence of a zero-temperature, CP-breaking transition at $\theta = \pi$ [81–85]; however, the interplay between chiral symmetry breaking and confinement can lead to a richer diagram, with the possibility of also considering quark chemical potentials or external fields [16–19,86–88].

There is one feature of the sketch in Fig. 13 which is pure speculation, stimulated by the analogy with the T-θ_B plane: the curve $T_c(\theta)$ hits the CP-breaking lines exactly at their end points, as it happens for $T_c(\theta_B)$ with the RW lines. If such speculation were correct, then, since $T_c(\theta)$ is first order at least for large N, it would be reasonable to assume that the end point of the CP lines is also first order, i.e., a triple point with two departing first-order lines, coinciding with the $T_c(\theta)$ line in the two adjacent branches. The picture could be modified by the presence of dynamical fermions because of the possible change in the order of the transition at $\theta = 0$ and the possible appearance of critical end points in the phase diagram. Unfortunately such a scenario is not easily testable by lattice simulations since, contrary to what happens for the T-θ_B plane, it regards a region affected by a severe sign problem.

IV. CONCLUSIONS

We have presented a discussion regarding the phase diagram of pure gauge SU(N) Yang-Mills theories in the presence of a topological θ term, based on both numerical

[2]The same approximation does not work in the low-T region because of infrared divergences.

[3]The evidence from Ref. [36], extracted by looking at higher-order cumulants of the topological charge distribution, is that the instanton gas approximation sets in around $T \sim 1.1 T_c$ for the SU(3) pure gauge theory.

results and considerations related to the large-N dependence of the theory.

First, we discussed the behavior of the deconfiment temperature as a function of θ, $T_c(\theta)$. The determination presented in Ref. [11], based on the method of analytic continuation from imaginary values of θ, has been improved by performing new simulations on a finer lattice with $N_t = 10$ (which confirms the continuum extrapolation of the curvature at $\theta = 0$ reported in Ref. [11]) and has been compared with new results obtained by reweighting configurations sampled at $\theta = 0$. As a result, we can conclude that systematic effects related to analytic continuation and to reweighting are under control, at least regarding the determination of the curvature of the critical line R_θ. The final, continuum value that we estimate for $N = 3$ is $R_\theta = 0.0178(5)$.

As a byproduct of our numerical analysis, we have explored the dependence of physical observables on the topological sector Q, showing that it is somewhat stronger around the transition, in particular for quantities directly related to deconfinement, like the Polyakov loop, and that the transition temperature itself can depend on the topological background. This may be a warning for lattice QCD studies performed in a fixed topological background.

Finally, in the last part of the paper, we have discussed the general features of the T-θ diagram. Most of the discussion has been inspired by the possible analogies and dualities (in the sense of an inversion of the low- and high-T regions) that exist—also from a large-N perspective—with the phase diagram of QCD in the presence of an imaginary baryon chemical potential. Periodicity in θ is smoothly realized in the high-T phase and is instead associated with a multibranched structure in the low-temperature phase, where the relevant dependence is on θ/N, implying first-order transitions which are met at odd multiples of $\theta = \pi$. Such transitions are the analogs of the Roberge-Weiss transitions in the high-T phase of QCD in the presence of an imaginary baryon chemical potential: in both cases the change in the realization of periodicity can be associated with a change in the relevant degrees of freedom, carrying (topological or baryon) charge 1 or $1/N$.

ACKNOWLEDGMENTS

We thank M. Anber, F. Bigazzi, G. Cossu, C. Bonati, F. Capponi, P. de Forcrand, E. S. Fraga, A. Di Giacomo, M. Mariti, M. Unsal, E. Vicari, and A. Zhitnitsky for many useful discussions. We acknowledge the use of the computer facilities of the INFN Bari Computer Center for Science, of the INFN-Genova Section and of the CSNIV cluster in Pisa. We thank the Galileo Galilei Institute for Theoretical Physics for the hospitality offered during the workshop "New Frontiers in Lattice Gauge Theories."

[1] E. Witten, Nucl. Phys. **156B**, 269 (1979).
[2] G. Veneziano, Nucl. Phys. **B159**, 213 (1979).
[3] C. Callan, R. Dashen, and G. Gross, Phys. Rev. D **17**, 2717 (1978).
[4] D. J. Gross, R. D. Pisarski, and L. G. Yaffe, Rev. Mod. Phys. **53**, 43 (1981).
[5] T. Schäfer and E. V. Shuryak, Rev. Mod. Phys. **70**, 323 (1998).
[6] A. Vilenkin, Phys. Rev. D **22**, 3080 (1980); D. Kharzeev, R. D. Pisarski, and M. H. G. Tytgat, Phys. Rev. Lett. **81**, 512 (1998); D. Kharzeev and A. Zhitnitsky, Nucl. Phys. **A797**, 67 (2007); D. E. Kharzeev, L. D. McLerran, and H. J. Warringa, Nucl. Phys. **A803**, 227 (2008); K. Fukushima, D. E. Kharzeev, and H. J. Warringa, Phys. Rev. D **78**, 074033 (2008).
[7] V. Azcoiti, G. Di Carlo, A. Galante, and V. Laliena, Phys. Rev. Lett. **89**, 141601 (2002).
[8] B. Alles and A. Papa, Phys. Rev. D **77**, 056008 (2008).
[9] S. Aoki, R. Horsley, T. Izubuchi, Y. Nakamura, D. Pleiter, P. E. L. Rakow, G. Schierholz, and J. Zanotti, arXiv:0808.1428.
[10] H. Panagopoulos and E. Vicari, J. High Energy Phys. 11 (2011) 119.
[11] M. D'Elia and F. Negro, Phys. Rev. Lett. **109**, 072001 (2012).
[12] M. D'Elia, M. Mariti, and F. Negro, Phys. Rev. Lett. **110**, 082002 (2013).
[13] M. Unsal, Phys. Rev. D **86**, 105012 (2012).
[14] E. Poppitz, T. Schfer and M. Unsal, J. High Energy Phys. 03 (2013) 087.
[15] M. M. Anber, arXiv:1302.2641.
[16] A. J. Mizher and E. S. Fraga, Nucl. Phys. **A831**, 91 (2009).
[17] H. Kouno, Y. Sakai, T. Sasaki, K. Kashiwa, and M. Yahiro, Phys. Rev. D **83**, 076009 (2011).
[18] Y. Sakai, H. Kouno, T. Sasaki, and M. Yahiro, Phys. Lett. B **705**, 349 (2011).
[19] T. Sasaki, J. Takahashi, Y. Sakai, H. Kouno, and M. Yahiro, Phys. Rev. D **85**, 056009 (2012).
[20] B. Alles, M. D'Elia, and A. Di Giacomo, Nucl. Phys. **B494**, 281 (1997); **B679**, 397(E) (2004); Phys. Lett. B, **412**, 119 (1997); Phys. Lett. B, **483**, 139 (2000); C. Gattringer, R. Hoffmann, and S. Schaefer, Phys. Lett. B **535**, 358 (2002).
[21] B. Lucini, M. Teper, and U. Wenger, Nucl. Phys. **B715**, 461 (2005).
[22] L. Del Debbio, H. Panagopoulos, and E. Vicari, J. High Energy Phys. 09 (2004) 028.
[23] R. Brower, S. Chandrasekharan, J. W. Negele, and U. J. Wiese, Phys. Lett. B **560**, 64 (2003).

[24] S. Aoki, H. Fukaya, S. Hashimoto, and T. Onogi, Phys. Rev. D **76**, 054508 (2007).
[25] G. Cossu, S. Aoki, H. Fukaya, S. Hashimoto, T. Kaneko, H. Matsufuru, and J.-I. Noaki, Phys. Rev. D **87**, 114514 (2013).
[26] E. Witten, Ann. Phys. (N.Y.) **128**, 363 (1980).
[27] N. Ohta, Prog. Theor. Phys. **66**, 1408 (1981); **67**, 993(E) (1982).
[28] E. Witten, Phys. Rev. Lett. **81**, 2862 (1998).
[29] I. E. Halperin and A. Zhitnitsky, Phys. Rev. D **58**, 054016 (1998).
[30] E. Witten, Adv. Theor. Math. Phys. **2**, 505 (1998).
[31] T. Sakai and S. Sugimoto, Prog. Theor. Phys. **113**, 843 (2005); **114**, 1083 (2005).
[32] O. Bergman and G. Lifschytz, J. High Energy Phys. 04 (2007) 043.
[33] A. Parnachev and A. R. Zhitnitsky, Phys. Rev. D **78**, 125002 (2008).
[34] A. R. Zhitnitsky, Nucl. Phys. **A813**, 279 (2008).
[35] A. S. Gorsky, V. I. Zakharov, and A. R. Zhitnitsky, Phys. Rev. D **79**, 106003 (2009).
[36] C. Bonati, M. D'Elia, H. Panagopoulos, and E. Vicari, Phys. Rev. Lett. **110**, 252003 (2013).
[37] M. G. Alford, A. Kapustin, and F. Wilczek, Phys. Rev. D **59**, 054502 (1999); A. Hart, M. Laine, and O. Philipsen, Phys. Lett. B **505**, 141 (2001); P. de Forcrand and O. Philipsen, Nucl. Phys. **B642**, 290 (2002); M. D'Elia and M.-P. Lombardo, Phys. Rev. D **67**, 014505 (2003).
[38] P. Cea, L. Cosmai, M. D'Elia, C. Manneschi, and A. Papa, Phys. Rev. D **80**, 034501 (2009); P. Cea, L. Cosmai, M. D'Elia, and A. Papa, Phys. Rev. D **81**, 094502 (2010); P. Cea, L. Cosmai, M. D'Elia, A. Papa, and F. Sanfilippo, Phys. Rev. D **85**, 094512 (2012).
[39] L. Del Debbio, H. Panagopoulos, and E. Vicari, J. High Energy Phys. 08 (2002) 044.
[40] M. D'Elia, Nucl. Phys. **B661**, 139 (2003).
[41] B. Alles, M. D'Elia, and A. Di Giacomo, Phys. Rev. D **71**, 034503 (2005).
[42] L. Giusti, S. Petrarca, and B. Taglienti, Phys. Rev. D **76**, 094510 (2007).
[43] E. Vicari and H. Panagopoulos, Phys. Rep. **470**, 93 (2009).
[44] M. Campostrini, A. Di Giacomo, and H. Panagopoulos, Phys. Lett. B **212**, 206 (1988).
[45] B. Berg, Phys. Lett. **104B**, 475 (1981); Y. Iwasaki and T. Yoshie, Phys. Lett. **131B**, 159 (1983); S. Itoh, Y. Iwasaki, and T. Yoshie, Phys. Lett. **147B**, 141 (1984); M. Teper, Phys. Lett. **162B**, 357 (1985); E.-M. Ilgenfritz, M. L. laursen, M. Müller-Preuβker, G. Schierholz, and H. Schiller, Nucl. Phys. **B268**, 693 (1986); M. Campostrini, A. Di Giacomo, H. Panagopoulos, and E. Vicari, Nucl. Phys. **B329**, 683 (1990).
[46] A. Di Giacomo and E. Vicari, Phys. Lett. B **275**, 429 (1992).
[47] G. Boyd, J. Engels, F. Karsch, E. Laermann, C. Legeland, M. Lutgemeier, and B. Petersson, Nucl. Phys. **B469**, 419 (1996).
[48] I. M. Barbour, S. E. Morrison, E. G. Klepfish, J. B. Kogut, and M.-P. Lombardo, Nucl. Phys. Proc. Suppl. A **60**, 220 (1998).
[49] Z. Fodor and S. D. Katz, Phys. Lett. B **534**, 87 (2002).
[50] E. Shuryak and T. Sulejmanpasic, arXiv:1305.0796.
[51] V. Azcoiti, A. Galante, and V. Laliena, Prog. Theor. Phys. **109**, 843 (2003).
[52] A. Roberge and N. Weiss, Nucl. Phys. **B275**, 734 (1986).
[53] M. D'Elia, F. Di Renzo, and M. P. Lombardo, Phys. Rev. D **76**, 114509 (2007).
[54] M. D'Elia and F. Sanfilippo, Phys. Rev. D **80**, 111501 (2009).
[55] P. de Forcrand and O. Philipsen, Phys. Rev. Lett. **105**, 152001 (2010).
[56] C. Bonati, G. Cossu, M. D'Elia, and F. Sanfilippo, Phys. Rev. D **83**, 054505 (2011).
[57] C. Bonati, P. de Forcrand, M. D'Elia, O. Philipsen and F. Sanfilippo, Proc. Sci., LATTICE (2011) 189.
[58] H. Kouno, Y. Sakai, K. Kashiwa, and M. Yahiro, J. Phys. G **36**, 115010 (2009).
[59] J. Braun, L. M. Haas, F. Marhauser, and J. M. Pawlowski, Phys. Rev. Lett. **106**, 022002 (2011).
[60] Y. Sakai, H. Kouno, and M. Yahiro, J. Phys. G **37**, 105007 (2010).
[61] G. Aarts, S. P. Kumar, and J. Rafferty, J. High Energy Phys. 07 (2010) 056.
[62] J. M. Pawlowski, AIP Conf. Proc. **1343**, 75 (2011).
[63] J. Rafferty, J. High Energy Phys. 09 (2011) 087.
[64] V. Pagura, D. G. Dumm, and N. N. Scoccola, Phys. Lett. B **707**, 76 (2012).
[65] K. Kashiwa, T. Hell, and W. Weise, Phys. Rev. D **84**, 056010 (2011).
[66] K. Morita, V. Skokov, B. Friman, and K. Redlich, Phys. Rev. D **84**, 076009 (2011).
[67] K. Nagata and A. Nakamura, EPJ Web Conf. **20**, 03006 (2012).
[68] L.-K. Wu and X.-F. Meng, Phys. Rev. D **87**, 094508 (2013).
[69] C. Vafa and E. Witten, Phys. Rev. Lett. **53**, 535 (1984).
[70] E. Witten, Nucl. Phys. **B149**, 285 (1979).
[71] V. A. Fateev, I. V. Frolov, and A. S. Shvarts, Nucl. Phys. **B154**, 1 (1979).
[72] B. Berg and M. Luscher, Commun. Math. Phys. **69**, 57 (1979).
[73] A. A. Belavin, V. A. Fateev, A. S. Schwarz, and Y. S. Tyupkin, Phys. Lett. **83B**, 317 (1979).
[74] T. C. Kraan and P. van Baal, Phys. Lett. B **435**, 389 (1998).
[75] F. Bruckmann, D. Nogradi, and P. van Baal, Nucl. Phys. **B666**, 197 (2003).
[76] F. Bruckmann, E. M. Ilgenfritz, B. V. Martemyanov, and P. van Baal, Phys. Rev. D **70**, 105013 (2004).
[77] D. Diakonov and V. Petrov, Phys. Rev. D **76**, 056001 (2007).
[78] M. Unsal and L. G. Yaffe, Phys. Rev. D **78**, 065035 (2008).
[79] A. Gorsky and V. Zakharov, Phys. Rev. D **77**, 045017 (2008).
[80] G. V. Dunne and M. Unsal, Phys. Rev. D **87**, 025015 (2013).
[81] R. F. Dashen, Phys. Rev. D **3**, 1879 (1971).
[82] P. Di Vecchia and G. Veneziano, Nucl. Phys. **B171**, 253 (1980).
[83] A. V. Smilga, Phys. Rev. D **59**, 114021 (1999).
[84] M. H. G. Tytgat, Phys. Rev. D **61**, 114009 (2000).
[85] M. Creutz, Phys. Rev. Lett. **92**, 201601 (2004); arXiv:1306.1245.
[86] M. A. Metlitski and A. R. Zhitnitsky, Phys. Lett. B **633**, 721 (2006); Nucl. Phys. **B731**, 309 (2005).
[87] D. Boer and J. K. Boomsma, Phys. Rev. D **78**, 054027 (2008).
[88] J. K. Boomsma and D. Boer, Phys. Rev. D **80**, 034019 (2009).